ELSEVIER

Journal of Alloys and Compounds 234 (1996) 244–250

Journal of ALLOYS AND COMPOUNDS

Structural characterisation of erbium silicide thin films on an Si(111) substrate

N. Frangis[a,1], G. Van Tendeloo[a], J. Van Landuyt[a,*], P. Muret[b], T.T.A. Nguyen[b]

[a] *Electron Microscopy for Materials Research (EMAT), University of Antwerp (RUCA), Groenenborgerlaan 171, B-2020 Antwerpen, Belgium*

[b] *Laboratoire d'Etudes des Propriétés Electroniques des Solides, CNRS, BP 166, 38042 Grenoble Cedex 9, France*

Received 29 September 1995

Abstract

$ErSi_{2-x}$ films ($x = 0.1$–0.3) grown by co-evaporation at different deposition ratios have been characterised by transmission electron microscopy, electron diffraction and high resolution electron microscopy. A very good epitaxial growth relation with the Si substrate was deduced for al samples and observed phases. Different defect modulated structures are formed; they can be described as structural variants (orthorhombic or rhombohedral) of the basic structure. The modulated phases are related to deviations from stoichiometry similar to crystallographic shear structures. The $ErSi_{1.9}$ material contains Si precipitates, illustrating the preference for the $ErSi_{1.7}$ composition to be maintained.

Keywords: Electron microscopy; Silicides; Modulated structures

1. Introduction

Rare earth (RE) silicides are of particular technological interest for electronic applications because of their metallic resistivity and the low Schottky barrier height on n-type silicon. They are candidates for use as low resistance ohmic contacts, as well as wide area infrared detectors [1,2]. Furthermore, the RE silicides are attractive since they crystallise in a hexagonal AlB_2 structure, with lattice parameters in the (0001) planes nearly matching those of the Si-(111) planes. During recent years several epitaxial growth methods for RE silicide thin films on (111) Si surface have been tried (see for example Refs. [3–8]). Electron microscopy characterisation of these materials is interesting from a technological point of view since the physical properties are often structurally related.

In the present work the structural characteristics of thin $ErSi_{2-x}$ films grown on Si are investigated by electron microscopy. The silicide thin films were grown by co-evaporation of Si and Er on a (111) Si substrate, followed by in-situ annealing at 750 °C. Three different types of sample were prepared: in type 1 the Si/Er ratio was 1.7, in type 2 it was 1.9–2, in type 3 the ratio was again 1.7 but on top of the silicide a thin Si film of 20 nm thickness was grown by MBE at 550 °C.

Specimens for cross-section electron microscopy were prepared using the traditional techniques, for example as described in Ref. [9].

2. Structural considerations

The $ErSi_2$ structure is hexagonal, of the AlB_2 type, with space group $P6/mmm$. The lattice parameters are $a_{hex} = 3.79 \pm 0.01$ Å and $c_{hex} = 4.085 \pm 0.005$ Å. The Er atoms are packed in simple hexagonal way and the Si atoms occupy the sites in the centre of the trigonal prisms formed by the Er atoms (Figs. 1(a), 1(b)) [10,11].

It is known from the literature that in the Er–Si system non-stoichiometric $ErSi_{2-x}$ ($0 \leq x \leq 0.5$) compounds can be formed. They contain vacancies randomly distributed on the Si sublattice, retaining the hexagonal structure, or have an ordered arrangement of vacancies, leading to the formation of several superstructures. The most stable compound is believed

* Corresponding author.

[1] On leave from the Department of Physics, Aristotle University of Thessaloniki, GR-540 06 Thessaloniki, Greece.

SSDI 0925-8388(95)02131-0

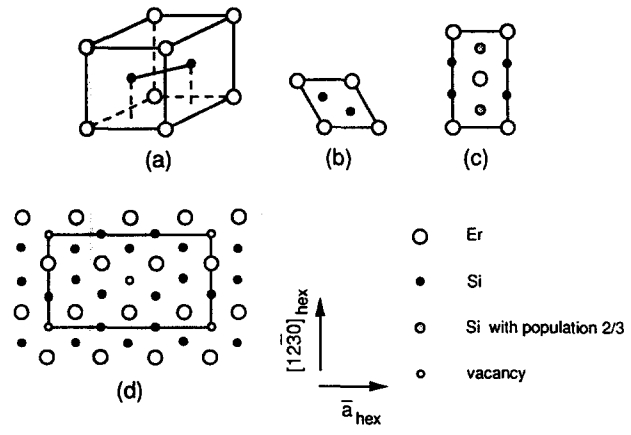

Fig. 1. (a) The basic hexagonal structure of $ErSi_2$ in space. Open and filled circles represent Er and Si atoms respectively. (b) Projection of the hexagonal structure along the $[0001]_{hex}$ axis. (c) Projection of the O_I structure along the $[0001]_{hex}$ axis. (d) Projection of the O_{II} structure along the $[0001]_{hex}$ axis with a hexagonal distribution of vacancies.

to be Er_3Si_5 or $ErSi_{1.67}$ ($x \simeq 0.33$), where one out six Si atoms is missing. The structure has been reported to be the basic hexagonal $ErSi_2$ structure (random distribution of vacancies) [12] or a partially ordered orthorhombic structure (hereafter called O_I), with lattice parameters $a_{O_I} = 6.54$ Å $\simeq a_{hex}\sqrt{3}$, $b_{O_I} = a_{hex}$, $c_{O_I} = c_{hex}$ and space group *Pmmm* [10,13]. In this structure the vacancies are randomly distributed over one of the two Si sites (Fig. 1(c)). Evidence has also been reported for a full ordering of the vacancies, giving rise to an orthorhombic structure (hereafter called O_{II}), with lattice parameters $a_{O_{II}} = 3a_{hex}$, $b_{O_{II}} = c_{hex}$, $c_{O_{II}} = a_{hex}\sqrt{3}$ and space group *Pmm*2 [7,13]. Two different distributions of the vacancies have been proposed for this structure, one retaining the hexagonal symmetry (Fig. 1(d)) and the other not. Finally, indications for the existence of other, longer period superstructures have also recently been reported by Arnaud d'Avitaya et al. [4] and Kaatz et al. [8].

3. Electron microscopy characterisation

3.1. General

Cross-section specimens for electron microscopy were prepared for all three types of sample. A Philips CM20 electron microscope was used for conventional microscopy and a Jeol 4000EX (400 kV) for the high resolution observations.

The silicide overlayer thickness is found to be in the range 15–30 nm. Samples of type 1 and 2 do not always have a smooth surface and show the presence of so-called pinholes. However, the interface between the Er silicide and the Si substrate is very sharp, although steps of a few atomic planes high are not exceptional (Figs. 2(a), 2(b)). In sample 3 the interface between the silicide and the Si substrate is often ill-defined (Fig. 2(c)), probably due to an interdiffusion between the two components. However, the interface between the silicide and the Si overlayer grown by MBE is of much better quality.

In the sample of type 2, on different sites, the silicide thin film is interrupted by islands of a material with a remarkably lighter contrast (see Fig. 3). Electron diffraction as well as high resolution EM enabled us to identify these islands as polycrystalline silicon, of which some grains are grown epitaxially on the substrate.

Electron diffraction patterns along the $[1\bar{2}30]_{hex} \equiv [01\bar{1}0]^*_{hex}$ zone axis, for the several phases present, are shown in Fig. 4. In all cases a very good epitaxial

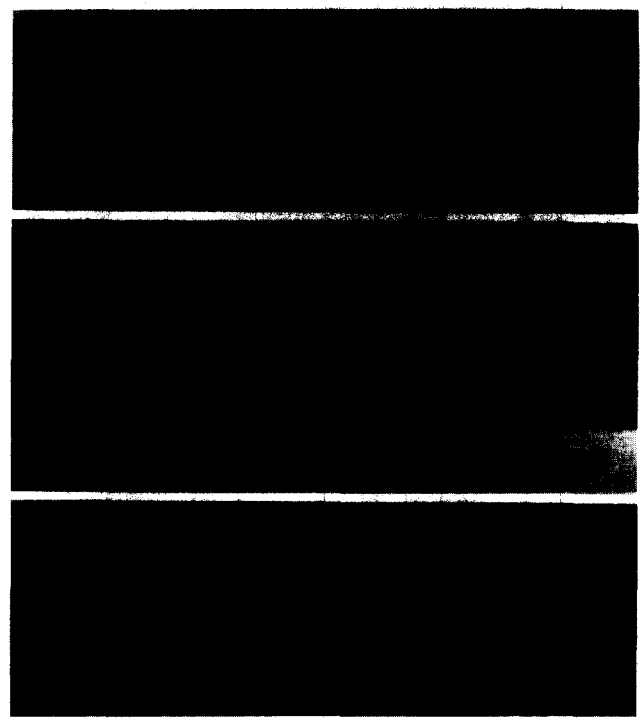

Fig. 2. Images of $ErSi_{2-x}$/Si thin films: (a) type 1, (b) type 2, (c) type 3. Arrows 1 indicate the presence of atomic steps at the silicide/Si interface. Arrows 2 indicate the presence of "grain boundaries". Note the presence of bands of a different "phase" (named A) in sample 1. In the Si–MBE overlayer of sample 3, stacking faults (SF) and twin interfaces (T) are detected. The axes indicated in (b) are valid for all three images.

Fig. 3. Low magnification image of sample 2 revealing the interruptions of the silicide identified as polycrystalline Si islands.

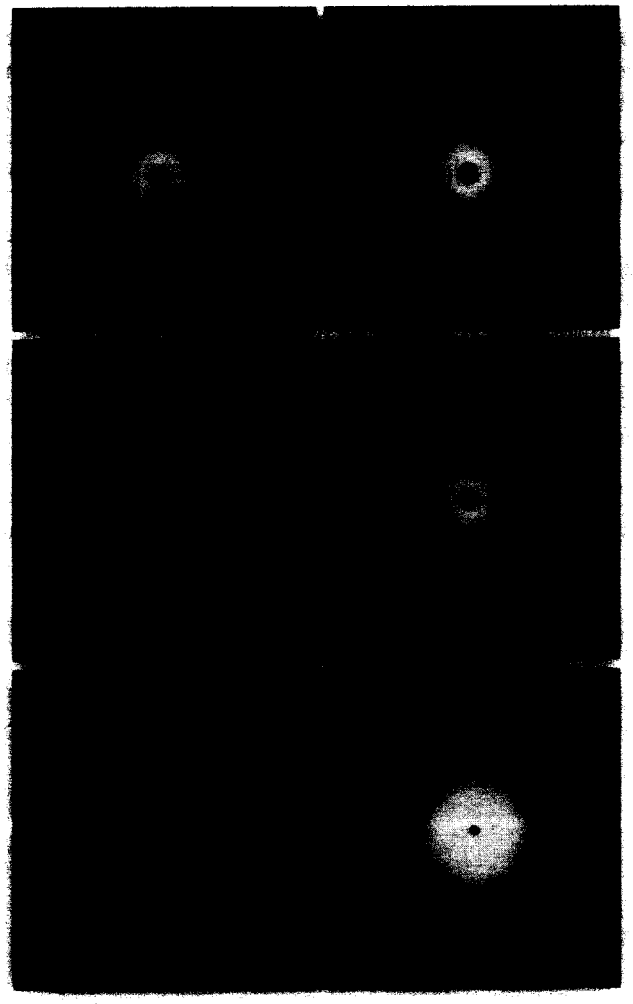

Fig. 4. Electron diffraction patterns along $[12\bar{3}0]_{hex}$ for several $ErSi_{2-x}$ phases (open and filled circles denote the $ErSi_2$ basic reflections and the Si reflections respectively). (a) The hexagonal basic structure; (b) the O_{III} structure; (c,d,e) incommensurate modulations; (f) the two arrays of brackets indicate the presence in the selected area of two periodicities, along the $[0001]_{hex}$, of 4.09 Å and 5.12 Å.

growth was found to exist. The Si substate reflections ([11$\bar{2}$] orientation) are always present. The silicide reflections, however, take different positions for different compositions, and actually reveal a number of commensurate and incommensurate modulated structures (Figs. 4(a)–4(f)). All of these patterns can be derived from the basic hexagonal pattern of Fig. 4(a). The following relations between the hexagonal silicide and the Si substrate are deduced: $[111]_{Si}//[0001]_{hex}$; $[1\bar{1}0]_{Si}//[10\bar{1}0]_{hex}$.

It is remarkable that, for different compositions, the basic a_{hex} parameter 3.82 ± 0.02 Å remains almost equal to the d_{110} Si parameter, which means that the former is slightly extended to allow for a perfect match between the two lattices.

The $[10\bar{1}0]$ zone axis patterns (Fig. 5) are similar for all compounds and only reveal a repeat distance

Fig. 5. Electron diffraction along the $[10\bar{1}0]_{hex}$ zone axis. Reflections due to twinning in the Si overlayer are also present.

$a_{hex}\sqrt{3}/2$ within the hexagonal interface plane. The $[12\bar{3}0]$ section is clearly the most instructive for revealing the characteristics of the modulated structures and studying the silicon vacancy ordering on the Si sublattice.

3.2. Basic commensurate structures

The two basic $[12\bar{3}0]$ diffraction patterns which are regularly observed are shown in Figs. 4(a) and 4(b). The most simple one (Fig. 4(a)) shows the presence of the basic $ErSi_2$-type reflections, compatible with the disordered hexagonal arrangement. This phase occurs in all samples studied. Another, related, basic pattern (Fig. 4(b)) is frequently observed. The corresponding structure can be described as orthorhombic (it will be termed O_{III} hereafter) and has lattice parameters $a_{O_{III}} = 3a_{hex}$, $b_{O_{III}} = \sqrt{3}a_{hex}$, $c_{O_{III}} = 2c_{hex}$.

Indications for the presence of this phase in Er–Si compounds have already been presented in Ref. [14].

In real space and projected along the viewing direction $[12\bar{3}0]$ both the O_{II} and O_{III} structures are schematically represented in Figs. 6(a) and 6(b). For O_{II} the partially vacant Si sites form a rectangular arrangement and can be formally described by an ...AAA... stacking along the c-axis. Note that in the $[10\bar{1}0]_{hex}$ projection (Fig. 6(d)) the separation between full and ordered vacancies containing Si columns is very small and impossible to distinguish by HREM. For the O_{III} structure (Fig. 6(b)) the c-axis is doubled due to a staggered arrangement of the Si vacancy columns; this structure can be described by an

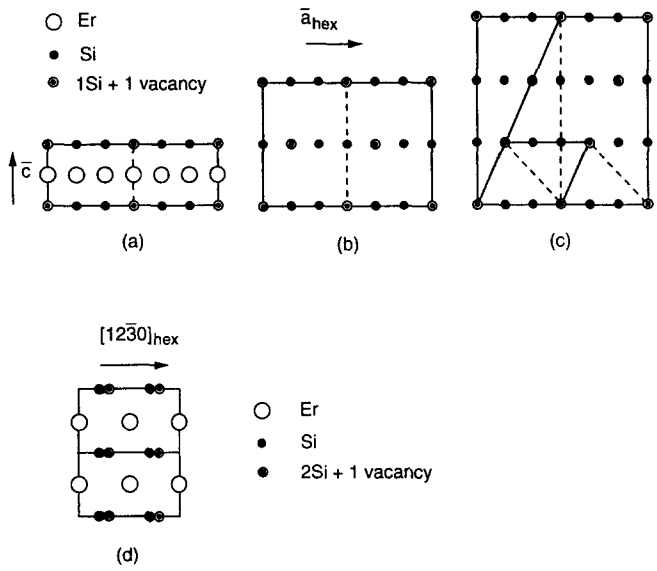

Fig. 6. Projection along the $a\sqrt{3}$ orthorhombic axis ($\equiv[12\bar{3}0]_{hex}$) for: (a) the O_{II} structure; (b) the O_{III} structure; (c) the 3R structure (for simplicity reasons the Er atoms are omitted in (b) and (c)). (d) Projection of the 3R structure along the $3a$ orthorhombic axis ($\equiv[10\bar{1}0]_{hex}$); this projection is identical for all the phases.

...ABAB... stacking along the c-axis. It can be considered as a long period structure (LPS) or a modulated structure based on the O_{II} structure by introducing alternately a displacement $\mathbf{R} = -[10\bar{1}0] = -1/3a_{O_{II}}$ and $-\mathbf{R} = [10\bar{1}0]$ every layer, or the equivalent to these vectors.

High resolution imaging of these phases is not straightforward, they are grown in thin films and are hard materials on a relatively soft substrate. The silicide film is therefore rather thick (not below 100 Å). Nevertheless, HREM images such as Fig. 7 allow the imaging code to be deduced; the Si layer is imaged as bright and the vacancy containing silicon columns appear as extra bright dots. In the lower part of Fig. 7 a doubling of the unit cell due to the presence of the O_{III} structure is clearly observed. Image simulations for a thickness of 400 Å confirm this intuitive interpretation. This imaging code will be the key for the interpretation of more complex structures and the explanation of the pseudo-incommensurate diffraction patterns of Figs. 4(c)–4(e).

3.3. Modulated structures

Since the O_{III} structure is derived from the "basic" O_{II} structure by a regular introduction of antiphase boundaries—or shear planes—along (0001), one can also derive other simple stacking sequences such as ...ABCABC...; this would then be a three layer (3R) rhombohedral sequence. The 3R structure is represented in Fig. 6(c), while its expected $[12\bar{3}0]_{hex}$ diffraction pattern for one and two variants is schematically represented in Figs. 8(a) and 8(b).

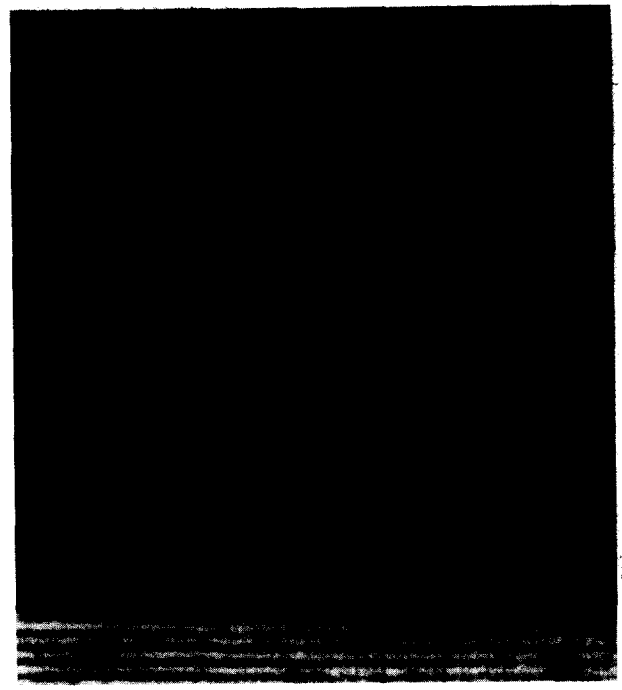

Fig. 7. High resolution image along the $[12\bar{3}0]_{hex}$ axis from an area containing mainly the O_{III} phase. A computer simulated image is included (thickness 400 Å, defocus −600 Å), the brightest dots correspond to vacancy containing Si columns.

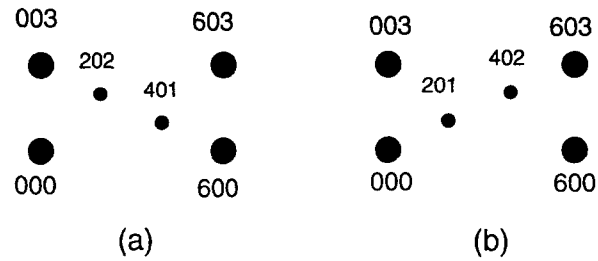

Fig. 8. Schematic representations of the expected electron diffraction patterns for the 3R structure along the $[12\bar{3}0]_{hex}$ axis for two twin related orientation variants.

Careful inspection of the "incommensurate" patterns of Figs. 4c–4e indicates that the superstructure reflections are situated close to the positions of this 3R phase. We will show that their structures can be derived from the 3R structure by a regular insertion of antiphase boundaries, not necessarily along the conservative (001) plane but along a non-conservative $(h0l)_o$ plane.

HREM images corresponding to the diffraction patterns 4(e) and 4(d) are reproduced as two examples in Figs. 9(a) and 11(a). The imaging code is the same as for the basic structures and the bright dots are to be associated with the vacancy containing Si columns. In Fig. 9(a) a monoclinic unit cell (14.1×12.4 Å^2) is outlined and the shear planes are indicated running parallel to the $(\bar{2}07)$ planes of the 3R structure.

The presence of these non-conservative APBs al-

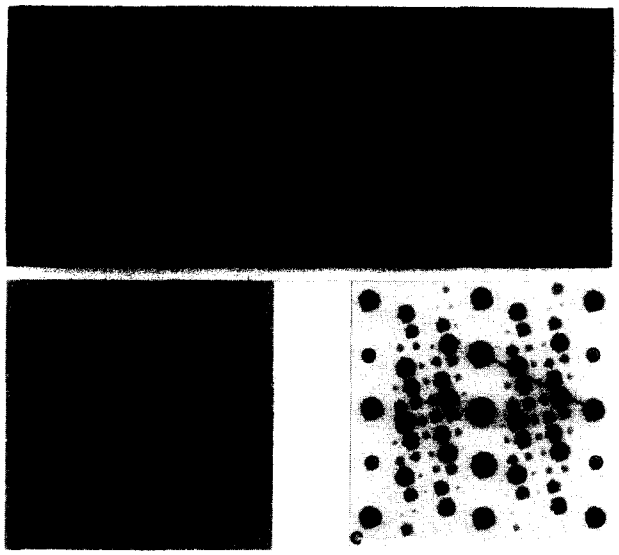

Fig. 9. (a) High resolution image along the $[12\bar{3}0]_{hex}$ axis from the first modulated structure phase. Arrows 1 indicate the planes of modulation, arrow 2 indicates the local existence of the 3R sequence of Fig. 6(c). A computer simulated image is included (thickness 400 Å, defocus −600 Å) to the left of a series of unit cells overdrawn on the image. (b) Computer Fourier transform of the above image. (c) Calculated diffraction pattern based on this model. The basic $ErSi_x$ reflections are encircled.

lows the local composition to deviate from the basic one. This effect is known in oxides and alloys, e.g. TiO_{2-x} [15] and $Au_{3\pm x}Mn$, and has been extensively described for $Au_{3+x}Mn$ alloys [16,17], where several modulated structures are found in the composition range between 20 and 25 at.% Mn (all deduced from the DO_{22} type structure by the introduction of non-conservative APBs). The orientation and density of the boundaries determine the local composition. Note that, as long as the shear plane has a conservative (001) orientation no compositional changes are to be expected and the derived stacking sequences can be termed polytypoids.

In Fig. 10(b) a schematic representation of a modulated structure, derived from the 3R structure (Fig. 10(a)) by the insertion of periodic APBs with a displacement vector $\mathbf{R} = 1/6[\bar{1}30]$ is shown. The unit cell of the new structure contains slightly less vacancies; the composition is estimated to be $ErSi_{1.68}$ instead of $ErSi_{1.67}$.

Based on the model of Fig. 10(b) image simulations have been performed and a calculated image is inserted in Fig. 9(a). The very good resemblance between the experimental and the calculated images, as well as with the unit cell of the projected structure indicated in Fig. 10(b), supports the validity of the proposed model. The Fourier spectrum of the HREM image is shown in Fig. 9(b) and the resemblance between this and the calculated diffraction pattern for the proposed superstructure (Fig. 9(c)) is striking. The

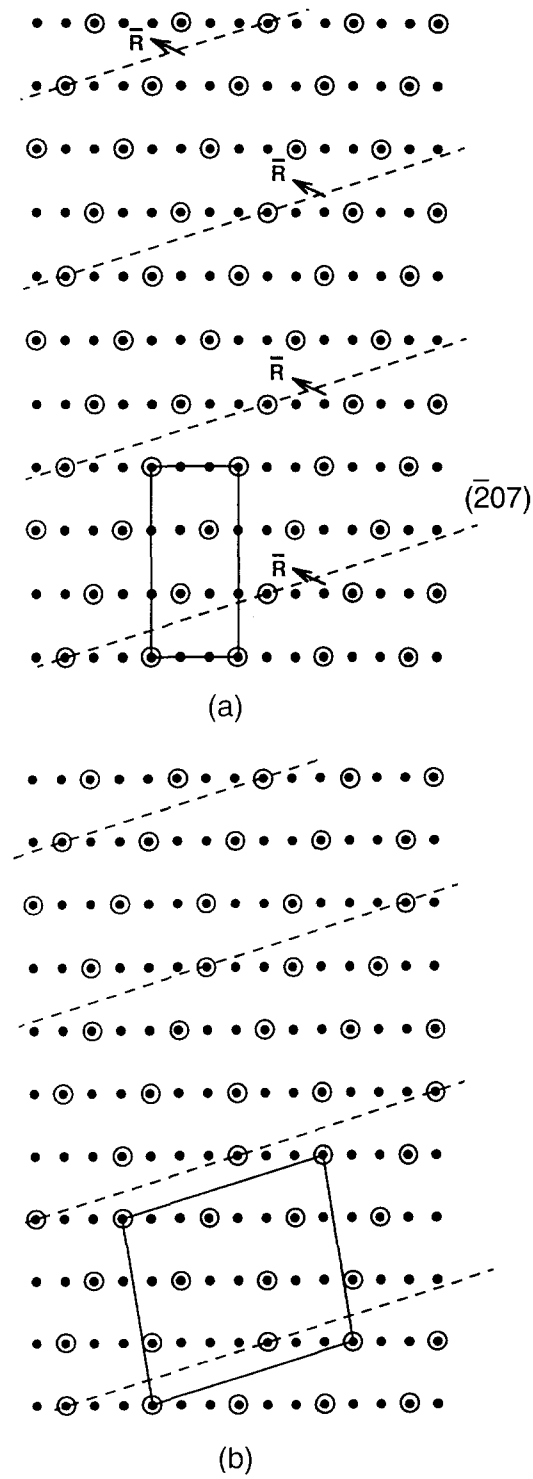

Fig. 10. The introduction of periodic shear planes in the 3R structure (a) gives rise to the first modulated structure (b). In both cases the unit cells are indicated.

two patterns present essentially the same features concerning the sites and relative intensities of the superstructure reflections. The slight differences are mainly introduced by the fact that the real structure is only observed over limited areas. Although at first the diffraction pattern (Fig. 4(e)) seems to correspond to

an incommensurate structure, the structure itself is a commensurate one; the incommensurate character is introduced by defects within this superstructure.

A HREM image of a different superstructure is reproduced in Fig. 11. Most of the shear planes are now (001), yielding an incommensurate modulated structure. Looking at grazing incidence along the basic 3R direction (arrow 2 in Fig. 11), the strongest dots are seen to form locally the 3R stacking sequence. Shifts of the rows over $\pm 1/6[100]$ are also observed and reveal the presence of APBs. As a result the local formation of the O_{III} structure can be easily recognised (unit cell indicated in the figure). The corresponding Fourier transform of the HREM image is shown in the inset to Fig. 11, revealing the incommensurate nature of this structure. The fact that the splitting is almost parallel to **c*** indicates that the "average" orientation of the shear planes is (001).

The positions of the reflections for a superstructure derived from a basic structure (3R) by the regular introduction of translation variants can also be derived by the fractional shift method [18]. The reciprocal space vectors **g** determining the series of new spots, in which a basic reflection **H** splits because of the periodic introduction of parallel shear planes with spacing d and shear vector **R**, are given by the formula

$$\mathbf{g} = \mathbf{H} + 1/d(m - \mathbf{H}\cdot\mathbf{R})\mathbf{e}$$

where m is an integer and **e** is the unit vector perpendicular to the interface.

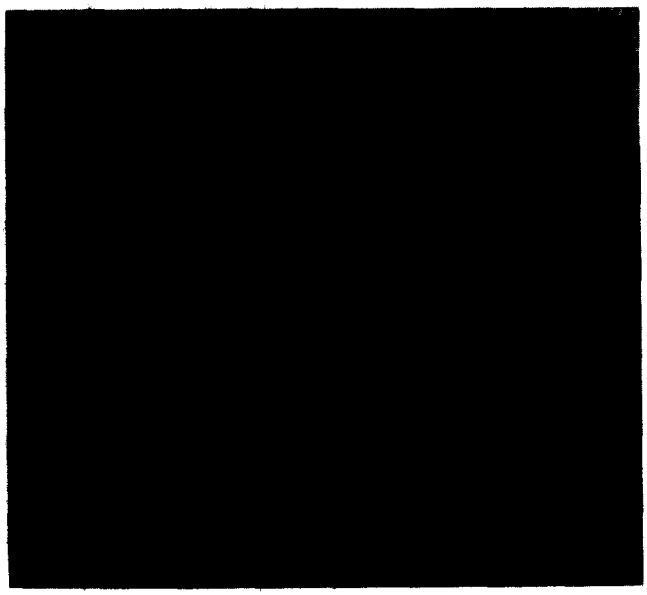

Fig. 11. A high resolution image taken along the $[12\bar{3}0]_{hex}$ axis from the second modulated structure phase. Arrows 1 indicate the shear planes and arrow 2 indicates the characteristic 3R direction. Some unit cells of the O_{III} structure are also indicated. The Fourier transform corresponding to the image is shown in the inset. The splitting of the spots is almost parallel to the **c***-axis. The distance between two successive superstructure spots is approximately 1/6[003]*.

In all the experimental electron diffraction patterns, as well as in the calculated patterns or the Fourier spectra, the fractional shifts of the extra spots relative to the positions of the 3R structure spots are found to be $\pm 1/3$. The more intense reflections being those with the smallest absolute values of fractional shift, as predicted by the theory. The fractional shifts are equal to $\mathbf{H}\cdot\mathbf{R}$. The shear vector with respect to the 3R structure can be written as $\mathbf{R} = \pm 1/6[\bar{1}30] = \pm[01\bar{1}0]_{hex}$. The displacement vector is also confirmed by HREM observations.

3.4. $(01\bar{1}0)$ planar interfaces

A different type of planar defect perpendicular to the interface and parallel to the $(01\bar{1}0)$ planes has also been observed, mainly in samples of type 3 (Fig. 12). HREM images taken with different defocus values

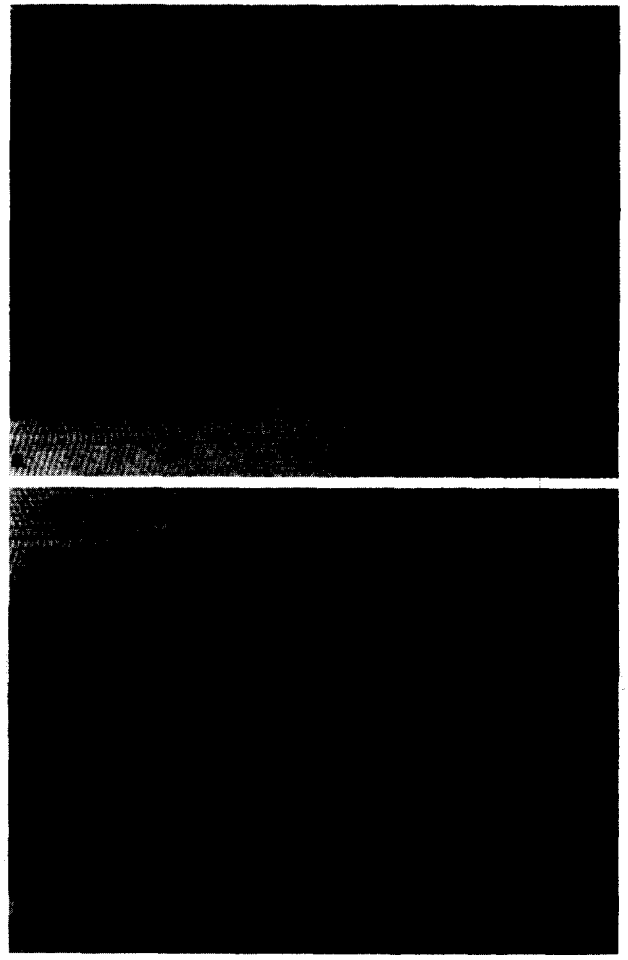

Fig. 12. High resolution images of the same area from a sample of type 3 taken along the $[10\bar{1}0]_{hex}$ axis with different defocus values. Four orientation variants are present, with boundaries (indicated by arrows) perpendicular to the silicide/Si interface. The image of (a) represents at higher magnification the area A of 2 (c). Note the different offsets of the rows in the two images.

show that the relative alignment of the horizontal bright dot rows across the vertical "interfaces" is very sensitive to focus. As can be seen from the image of Fig. 12(b), a shift between the rows of the two "grains" is present, although it is not in the image of Fig. 12(a) taken with a different defocus value. This observation, together with the difference in background intensity, indicate that these interfaces are "twin" planes separating orientation variants of the O_{III} superstructure based on a common Er sublattice. Indeed, three orientation variants can exist depending on which of the three equivalent hexagonal directions, $[10\bar{1}0]$, $[01\bar{1}0]$, $[1\bar{1}00]$, becomes the $a_{O_{III}}$ orthorhombic axis. All three orientation variants have the same structure projection and image for a perfect zone axis alignment; however, small deviations in thickness or defocus value or a slight tilt away from the perfect orientation, will all affect the position of the rows of bright dots as observed in Figs. 12(a) and 12(b).

In some diffraction patterns reflections appear which correspond to a repeat distance of about 5.12 Å along the c-axis (Fig. 4(f)). In the real space images (Fig. 2(a)) the corresponding "phase" appears as bands between the phases just described. The interplanar distance of 5.12 Å equals the d_{101} of the O_{III} phase. It is therefore acceptable that this "phase" consists in fact of bands of the O_{III} phase, misoriented with respect to the normal thin film, in such a way that the $[10\bar{1}1]^*$ axis is now parallel to the $[111]^*_{Si}$ axis. Unfortunately, the high resolution images do not provide further information because of the limited resolution of the available instrument.

4. Conclusions

Electron microscopy of erbium silicide thin films grown under slightly different conditions on silicon (111) substrates enabled us to characterise these layers to present a very good epitaxial growth for all samples and for all observed phases. Ordering of vacancies in the silicon sublattice seems to be the most dominant reason for the formation of different superstructures within a common Er sublattice.

A more homogeneous composition for the $ErSi_{2-x}$ systems is observed for the $x = 0.3$ silicide. It is remarkable that for higher concentrations of Si the formation of Si islands was found; these lower the Si content in the silicide down to the composition $ErSi_{1.7}$, which appears the most stable one.

The presence of several "incommensurate" phases in this material can be attributed to non-stoichiometry, as confirmed by electron diffraction and HREM studies. At the non-conservative interfaces the concentration of vacancies deviates from that in the bulk and a crystallographic shear-type structure is formed. Structural models for these new phases are derived.

Acknowledgements

This paper reports results obtained within the HCM program ERBCHRXRT 930355 supported by the EC. One of us (N.F.) has also carried out the work as part of a Community Training Project financed by the Commission (Contract no. ERBCHBICT 941798).

References

[1] P.L. Janega, J. McCaffrey and D. Landheer, *Appl. Phys. Lett.*, *55* (1989) 1415.
[2] L. Pahun, Y. Campidelli, F. Arnaud d'Avitaya and P.A. Badoz, *Appl. Phys. Lett.*, *60* (1992) 1166.
[3] J.A. Knapp and S.T. Picraux, *Appl. Phys. Lett.*, *48* (1986) 466.
[4] F. Arnaud d'Avitaya, A. Perio, J.-C. Oberlin, Y. Campidelli and J.A. Chroboczek, *Appl. Phys. Lett.*, *54* (1989) 2198.
[5] F.H. Kaatz, M.P. Siegal, W.R. Graham, J. Van Der Spiegel and J.J. Santiago, *Thin Solid Films*, *184* (1990) 325.
[6] C. D'Anterroches, P. Perret, F. Arnaud d'Avitaya and J.A. Chroboczek, *Thin Solid Films*, *184* (1990) 349.
[7] M.-H. Tuilier, C. Pirri, P. Wetzel, G. Gewinner, J.-Y. Veuillen and T.A. Nguyen Tan, *Surf. Sci.*, *307–309* (1994) 710.
[8] F.H. Kaatz, W.R. Graham and J. Van der Spiegel, *Appl. Phys. Lett.*, *62* (1993) 1748.
[9] A. Romano, J. Vanhellemont, H. Bender and L. Rossou, *Mater. Res. Soc. Symp. Proc.*, *115* (1988) 183.
[10] V. Ghetta, E. Houssay, A. Rouault, R. Madar and B. Lambert, *C.R. Acad. Sci. Paris, Ser. II*, *309* (1989) 995.
[11] W.B. Pearson, *The Crystal Chemistry and Physics of Metals and Alloys*, Wiley Interscience, New York, 1972, p. 492.
[12] A. Iandelli, A. Palenzona and G.L. Olcese, *J. Less-Common Met.*, *64* (1979) 213.
[13] S. Auffret, J. Pierre, B. Lambert, J.L. Soubeyroux and J.A. Chroboczek, *Physica B*, *162* (1990) 271.
[14] D.B.B. Lollman, *These Docteur*, Universite Joseph Fourier-Grenoble I, 1992, p. 133.
[15] J. Van Landuyt, *J. De Physique, Coll. C7, Suppl. 12, 35* (1974) C7.
[16] G. Van Tendeloo and S. Amelinckx, *Phys. Status Solidi A*, *65* (1981) 73.
[17] G. Van Tendeloo and S. Amelinckx, *Phys. Status Solidi A*, *65* (1981) 431.
[18] J. Van Landuyt, R. De Ridder, R. Gevers and S. Amelinckx, *Mater. Res. Bull.*, *5* (1970) 353.